Available online at www.sciencedirect.com
ScienceDirect
International Journal of Thermal Sciences 47 (2008) 355–368
International Journal of Thermal Sciences
www.elsevier.com/locate/ijts

Interaction between natural convection and surface thermal radiation in tilted slender cavities

R. Alvarado [a,1], J. Xamán [a,*], J. Hinojosa [b,2], G. Álvarez [a,1]

[a] *Centro Nacional de Investigación y Desarrollo Tecnológico, CENIDET-DGEST-SEP, Prol. Av. Palmira s/n, Col. Palmira, Cuernavaca, Morelos, C.P. 62490, Mexico*

[b] *Universidad de Sonora, Blvd. Luis Encinas y Rosales, Col. Centro, Hermosillo, Sonora, C.P. 83000, Mexico*

Received 16 May 2006; received in revised form 10 February 2007; accepted 12 March 2007

Available online 7 May 2007

Abstract

In this paper a numerical investigation of the interaction between two modes of heat transfer, natural convection and surface thermal radiation, in a tilted slender cavity is studied. The bottom and top surfaces of the cavity are heated and cooled at constant temperatures, while its sidewalls remain thermally insulated. The studied parameters are: the Rayleigh number ($10^4 \leqslant Ra \leqslant 10^6$), the aspect ratio ($8 \leqslant A \leqslant 16$) and the inclination angle ($15° \leqslant \lambda \leqslant 35°$). The steady state 2-D governing equations have been solved by the finite volume method. All the inner surfaces are assumed to be gray diffuse emitters and reflectors of radiation. The numerical model was reduced and compared to cases reported in the literature finding a good agreement. Streamlines, isotherms and total Nusselt numbers as a function of Rayleigh number for different inclinations are presented. The interaction between the two modes of heat transfer reveals that the decoupling of two mechanisms of heat transfer is not possible; the performance of the flow patterns, the isotherms and the radiative behavior on the walls was different for the uncoupled and coupled modes of heat transfer in the tilted slender cavity. The steady state results indicated that the radiative surface radiation coupled with natural convection modifies appreciably the flow patterns and the average heat transfer in the slender cavity. The total heat transfer increases when the inclination angle increases, except when the flow structure changes from the multi-cell to the unit-cell pattern. However, the total heat transfer decreases when the aspect ratio increases. A comprehensive correlation for the total Nusselt number has been proposed.

Keywords: Natural convection; Tilted cavities; Rectangular enclosures; Radiative exchange

1. Introduction

Coupled natural convection and radiation transport processes in cavities arise in many engineering applications, such as solar energy collectors, cooling of electronic devices, multilayered walls (façades) and double windows, etc. The phenomenon of heat transfer in a cavity is as varied as the geometry and orientation of the enclosure. In the literature review the enclosure phenomena can be classified as: (1) vertical and inclined cavities heated from the side and (2) horizontal enclosures heated from below. In cavities heated from the side, the problem of natural convection in square cavities heated differentially with adiabatic top and bottom walls has become the classical research problem extensively studied by experimental, analytical and numerical methods to get a better understanding of the governing processes [1–3]. In other geometries and orientations, natural convection in rectangular cavities for various aspect ratios also has been studied extensively; for example, Ozoe et al. [4,5] dealt with the problem of natural convection in inclined rectangular channels heated on one side and cooled on the opposing side. Their results indicated that as the angle of inclination increased a minimum and then a maximum heat transfer occurred, also, they found out that, the angle of inclination was a strong function of the aspect ratio and a weak function of the Rayleigh number. Later, Rahman and Sharif [6]

* Corresponding author. Tel./fax: +52 (777) 3 62 77 70.
E-mail addresses: robertoalvaradoj@gmail.com (R. Alvarado), jxaman@cenidet.edu.mx (J. Xamán), fhinojosa@iq.uson.mx (J. Hinojosa), gaby@cenidet.edu.mx (G. Álvarez).
[1] Tel./fax: +52 (777) 3 62 77 70.
[2] Tel./fax: +52 (662) 2 59 21 05.

1290-0729/$ – see front matter
doi:10.1016/j.ijthermalsci.2007.03.007

Nomenclature

A	aspect ratio (L/H)	
C_p	specific isobaric heat capacity	$\mathrm{J\,kg^{-1}\,K^{-1}}$
F_{Aj-Ak}	view factor between elements $j-k$	
g	gravitational acceleration, 9.81	$\mathrm{m\,s^{-2}}$
H	height of the cavity	m
L	length of the cavity	m
Nu	Nusselt number	
P	pressure	Pa
Pr	Prandtl number (ν/α)	
q	heat flux	$\mathrm{W\,m^{-2}}$
Ra	Rayleigh number $(g\beta\Delta T H^3/\nu\alpha = Gr\,Pr)$	
T	temperature	K
T_0	reference temperature $[(T_h+T_c)/2]$	K
u, v	velocity components	$\mathrm{m\,s^{-1}}$
x, y	Cartesian coordinates	m

Greek symbols

α	thermal diffusivity	$\mathrm{m^2\,s^{-1}}$
β	thermal expansion coefficient	$\mathrm{K^{-1}}$
ΔT	temperature difference	K
ε	emissivity	
κ	thermal conductivity	$\mathrm{W\,m^{-1}\,K^{-1}}$
λ	inclination angle	°
μ	dynamic viscosity	$\mathrm{kg\,m^{-1}\,s^{-1}}$
ν	kinematic viscosity	$\mathrm{m^2\,s^{-1}}$
ρ	density	$\mathrm{kg\,m^{-3}}$
ρ^*	reflectivity	
σ	Stefan–Boltzmann constant, $5.670\times10^{-8}\,\mathrm{W\,m^{-2}\,K^{-4}}$	
$\tau_{xx}, \tau_{xy}, \tau_{yy}$	stress	Pa

Subscripts

c	cold wall
cond	conductive
conv	convective
E	adiabatic right wall
h	hot wall
in	inlet
j	jth element
k	kth element
N	isothermal top wall at T_c
out	outlet
rad	radiative
S	isothermal bottom wall at T_h
total	total quantities
W	adiabatic left wall

studied the laminar natural convection in differentially heated inclined rectangular enclosures of aspect ratios from 0.25 to 4. They considered a rectangular cavity with and without internal heat generation showing that the uniform internal heat generation increases the local heat flux ratio along the hot wall and decreases it along the cold wall. They also found that the convection strength increases as the aspect ratio increases. They mention that shallow or high aspect ratio enclosures are used for solar collectors because minimum heat loss by convection is required. From the previous literature, we can see that the contribution due to surface radiation is either absent or ignored.

Other studies considered the effect that surface radiation has on natural convection, but they are focused mainly in square cavities. In cavities heated from the side, combined natural convection, conduction and radiation in a square cavity with opaque walls with a high temperature source, appear in the work of Larson and Viskanta [7], they found that the radiation dominates the heat transfer in the enclosure and alters the convective flow patterns significantly. Recently, Chang et al. [8], Balaji and Venkateshan [9], Akiyama and Chong [10], Mahpatra et al. [11] and Ramesh and Venkateshan [12] studied numerically and experimentally the radiation and natural convection interaction phenomena in differentially heated square cavities. Chang et al. in 1983 considered equal vertical finite-thickness partitions located at the centers of the ceiling and floor of the square cavity; they showed that for empty square enclosures, the effect of radiation is the increase of the bulk temperature of the gas in the enclosure and for partitioned enclosures, the partition provides an effective means to block the radiation exchange and also to increase the internal resistance for the convective flow. Comprehensive correlations for convection and radiation based on the numerical calculation of the coupled problem were given by Balaji and Venkateshan in 1994. Later on, gray surfaces and the variation of the emissivities in the cavity were studied by Akiyama and Chong in 1997, they showed that surface radiation significantly altered the temperature distribution and that the Nusselt number increases with the increase of Ra number. In 1999, Mahpatra et al., considered the variable property laminar natural convection finding that the presence of radiation destroys the thermal stratification in the core of the cavity. In 1999, Ramesh and Venkateshan presented an experimental study, clearly showing the influence of surface radiation when suppressing the natural convection for all walls highly polished (highly emissive walls). In cavities heated from below, Soong et al. [13] studied the mode transition and reported that a hysteresis phenomenon appears for $As = 4$ and $Ra > 2000$. Later, a transient study showing the effect of the inclination angle on the surface radiation is reported by Tzeng et al. [14]; the study revealed that at some critical situations, natural convection in inclined enclosures is very sensitive to the change of tilt angle. Recently, Ridouane et al. [15] studied the effect of surface radiation on natural convection in square cavities heated from below. Their results indicated that, the surface radiation alters significantly the existence range of the solution and the average heat transfer through the horizontal walls of the cavity. It was found that, for a fixed Ra, the global heat transfer across the enclosure depends only on the magnitude of the emissivity of the active walls. In the same year, a three dimensional numerical study of the interaction between radiation and natural convection in a differentially heated cu-

bic cavity considering both transparent and participating media was reported by Colomer et al. [16]. They made a comparison between the 3-D simulations and the 2-D results, finding a good agreement between both solutions which means that the effect of the end walls is small. Also, their results indicated that, in a transparent medium, the radiation significantly increases the heat flux. Currently, Ridouane et al. [17] reported the effects of radiation on natural convection in a Rayleigh–Benard square enclosure with unsteady conditions. The simulations were done for two values of the emissivities of the active and insulated walls (0.05 and 0.85). The results showed periodic solutions during the transition from the bicellular flows to the unicellular flow. The authors concluded that the nature and the magnitude of these periodic solutions are highly affected by the walls emissivity and the type of the bicellular steady-state solution.

Very few numerically studies considered the interaction of surface radiation on natural convection for shallow or high aspect ratio enclosures. The problem of decoupling or coupling radiation arises, due to the effect of the dimension of the top and bottom walls on the side walls. Balaji and Venkateshan [18] made a detailed numerical study of combined surface radiation and free convection problem at essentially low moderate temperature levels for cavities with aspect ratios in the range of 2–20. The purpose of the study was to give correlations for both convective and radiative heat transfer across the cavity. They say that, even under severe case of emissivity of all the walls close to 1 at such temperature levels, the temperature profile in the top and bottom walls are dominated by convection and not by radiation. Under this condition the coupling between radiation and free convection at the top and bottom walls does not significantly affect the radiation heat transfer itself. However, Velusamy et al. [19] made a numerically study of the interaction effects of surface radiation with turbulent natural convection of a transparent medium in rectangular enclosures, covering a wide range of *Ra* numbers from 10^9 to 10^{12} and aspect ratios of 1–200. They obtained solutions by considering convection–radiation coupling as well as by neglecting this coupling. In the later case, convective and radiative heat transfers are estimated totally independent of each other. They mention that for square enclosures, the decoupled analysis under predicts the heat transfer rate and the convective–radiative coupling becomes weaker as the aspect ratio increases in tall enclosures.

The above literature review shows that the effect of the inclination angle on natural convection in square and slender cavities has been studied, but the effect of the inclination angle on the interaction between surface radiation and natural convection is mostly related with square cavities. In the work reported herein, our objective is to present the effect of the inclination angle on the thermal performance of tilted slender cavities heated from a side by considering the interaction between the decoupled and coupled surface radiation and natural convection for $10^4 \leqslant Ra \leqslant 10^6$, aspect ratios of 8, 12 and 16, and inclination angles range from 15°to 35°. The Nusselt number correlation obtained may be used for better solar collector's design in latitudes locations between 35° and 15°, because, most of the heat losses are from the top of the collector [20].

2. Problem statement

2.1. Physical model

A rectangular cavity with a length L and a height H considered in this study is shown in Fig. 1. Two sidewalls are thermally insulated, and the other walls are heated and cooled at constant temperatures T_h and T_c, respectively. Air inside the cavity is considered ($Pr = 0.708$). Steady state and laminar flow is considered. The Rayleigh numbers are between $10^4 \leqslant Ra \leqslant 10^6$, and the aspect ratios of 8, 12 and 16 are considered in the computations. All physical properties are assumed constant at a reference temperature of $T_0 = 330$ K, and the Boussinesq approximation is assumed. All walls are assumed to be gray diffuse emitters and reflectors of thermal radiation. The inclination angles are in the range of 15°–35°. Table 1 shows the dimensions (length L and height H) for different aspect ratios and the Rayleigh numbers considered in this study. Others parameters selected are $\Delta T = 47$ K (which corresponds to the temperature difference between the absorber plate, T_h, and the glass cover, T_c, in solar collectors) and the surface emissivities $\varepsilon_N = 0.850$, $\varepsilon_S = 0.975$ and $\varepsilon_E = \varepsilon_W = 0.900$; which correspond to the glass surface, the black paint and the insulating materials respectively for typical solar collectors [21].

2.2. Governing equations

The steady state governing equations for 2-D, incompressible and laminar flows are the conservation of mass, momentum and energy equations:

$$\frac{\partial(\rho u)}{\partial x} + \frac{\partial(\rho v)}{\partial y} = 0 \tag{1}$$

$$\frac{\partial(\rho u \cdot u)}{\partial x} + \frac{\partial(\rho v \cdot u)}{\partial y} = -\frac{\partial P}{\partial x} + \frac{\partial}{\partial x}(\tau_{xx}) + \frac{\partial}{\partial y}(\tau_{xy}) + \rho g \beta (T - T_0)\sin\lambda \tag{2}$$

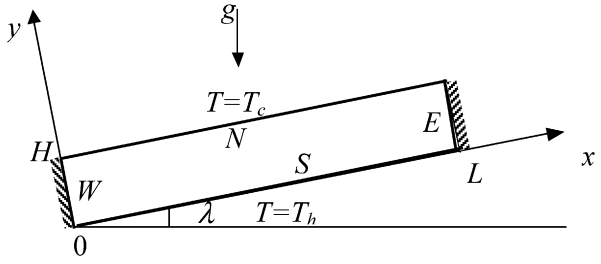

Fig. 1. Physical model of the cavity.

Table 1
Rayleigh numbers and equivalent cavity dimensions

Ra	*H* (m)	*L* (m)		
		$A = 8$	$A = 12$	$A = 16$
1×10^4	0.015	0.121	0.181	0.242
1×10^5	0.032	0.261	0.391	0.522
1×10^6	0.070	0.562	0.843	1.125

$$\frac{\partial(\rho u\cdot v)}{\partial x}+\frac{\partial(\rho v\cdot v)}{\partial y}$$
$$=-\frac{\partial P}{\partial y}+\frac{\partial}{\partial x}(\tau_{yx})+\frac{\partial}{\partial y}(\tau_{yy})+\rho g\beta(T-T_0)\cos\lambda \quad (3)$$

$$\frac{\partial(\rho C_p u\cdot T)}{\partial x}+\frac{\partial(\rho C_p v\cdot T)}{\partial y}=\frac{\partial}{\partial x}\left[k\frac{\partial T}{\partial x}\right]+\frac{\partial}{\partial y}\left[k\frac{\partial T}{\partial y}\right] \quad (4)$$

2.3. Boundary conditions

The non-slip condition is applied for the hydrodynamic boundary conditions at the solid walls ($u=v=0$). Two opposite walls are maintained at constant temperatures ($T=T_h$ for $y=0$, $T=T_c$ for $y=H$, with $T_c<T_h$). While the other two are adiabatic: $-k\frac{\partial T}{\partial x}+q_{\text{rad}}=0$ for $x=0$ and

$$k\frac{\partial T}{\partial x}-q_{\text{rad}}=0 \quad \text{for } x=L$$

2.4. Net radiation method

The radiative heat flux for the jth element on each wall is given by the following energy balance:

$$q_{\text{rad}\,j}=q_{\text{out}\,j}-q_{\text{in}\,j} \quad (5)$$

where the radiosity for the jth element is defined as:

$$q_{\text{out}\,j}=\varepsilon_j\sigma T_j^4+\rho_j^* q_{\text{in}\,j} \quad (6)$$

the irradiation is given by:

$$q_{\text{in}\,j}=\sum_{k=1}^{m}\int_{A_k} q_{\text{out}\,k}F_{Aj-Ak} \quad (7)$$

where the summation over the surface element k is to be taken for all the elements of the boundary with which j can interact radiatively.

2.5. Heat transfer

The total heat transfer across the hot wall is given by the Nusselt numbers. The total heat transfer involves the contribution of the convective and radiative Nusselt numbers. Thus, the total, convective and radiative Nusselt numbers can be expressed as by Akiyama and Chong [10]:

$$Nu_{\text{total}}=Nu_{\text{conv}}+Nu_{\text{rad}} \quad (8)$$

where:

$$Nu_{\text{conv}}=\frac{-k}{q_{\text{cond}}}\int_0^L\frac{\partial T}{\partial y}\,\mathrm{d}x \quad (9)$$

$$Nu_{\text{rad}}=\frac{1}{q_{\text{cond}}}\int_0^L q_{\text{rad}}\,\mathrm{d}x \quad (10)$$

$$q_{\text{cond}}=k(T_h-T_c)/W \quad (11)$$

3. Numerical procedure

The governing equations (1)–(4) were solved by the finite-volume method suggested by Patankar [22]. A non-uniform staggered grid was used, which was built using tangent hyperbolic functions. Thin grids were considered next to the boundary layers. The convection terms were approximated by a hybrid scheme and the diffusive terms by central space differences. The SIMPLEC algorithm [23] was used to couple continuity and momentum equations. The resulting algebraic equation system was solved using the Line Gauss–Seidel Alternating Direction Implicit (LGS-ADI) method. Underrelaxation was considered. In order to obtain good convergence solutions, the convergence criterion for the residuals was set at 1×10^{-10}. In the coupling between natural convection and surface thermal radiation at the boundaries, the radiative balance at the walls was solved using an iterative approach. The view factors between the elements were determined by the Hottel's crossed string method; since the view factors are only a function of the geometry, their calculation was performed before the beginning of the main iteration procedure. The radiosity equations were solved by the Simpson's rule [21].

The general procedure can be summarized in the following steps:

(1) Initial guess values of temperature and velocities in the cavity were given.
(2) Eqs. (5)–(7) were computed in order to get the local radiative heat flux on the walls.
(3) The pressure–velocity was calculated by the SIMPLEC algorithm.
(4) With the new calculated values of local radiative heat flux and velocity, the temperature field in the cavity was obtained.
(5) A convergence criterion was applied and
(6) the process was repeated until the convergence criterion was achieved.

The accuracy of the numerical results was checked through numerous tests on the grid size effect. The grids used were 176×31, 176×41, 176×51, 176×61, 101×41, 126×41, 151×41, 176×41 and 201×41 for $Ra=10^6$, $A=16$ and $\lambda=15^\circ$ for surface radiation coupled with the natural convection flow. Based on the numerical experiments, the computational grid that renders grid independent solutions was 176×41. Therefore, a 176×41 grid was used for all cases herein considered. The computer numerical simulations were performed on a PC Lanix, Pentium 4, CPU 2.42 GHz, RAM of 256 MB and 60 GB on HDD.

3.1. Verification

In order to verify the numerical code, the numerical model was reduced to the classical case of natural convection and surface thermal radiation in a square cavity heated from below, reported in the work of [15]. The convective and radiative Nusselt numbers of the hot wall were compared with the ones

Table 2
Comparison between the present study and the reported results in the literature of natural convection and radiation in a square cavity

	Ra	ε	Nu_{conv}	Nu_{rad}	Nu_{total}
Ridouane et al. [15]	2×10^6	0	7.617	0	7.617
Present study			7.665 (0.63%)	0	7.665 (0.63%)
Ridouane et al. [15]	10^6	0.5	6.267	6.599	12.866
Present study			6.107 (2.56%)	6.249 (5.31%)	12.356 (3.97%)
Ridouane et al. [15]	4×10^5	1	4.722	11.462	16.183
Present study			4.591 (2.78%)	10.871 (5.16%)	15.462 (4.46%)

Note. The values in ( ) are the absolute difference in %.

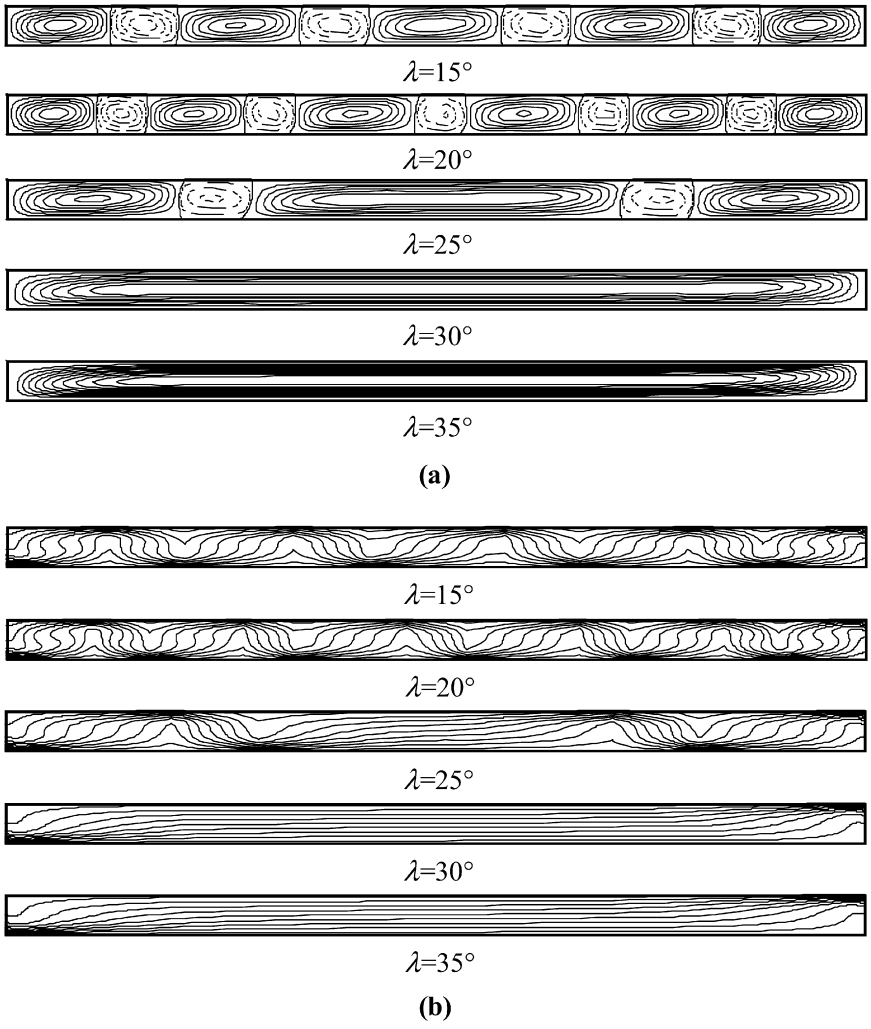

Fig. 2. Case uncoupled—streamlines (a) and isotherms (b) for a cavity of $A = 16$, $Ra = 10^4$ for $\lambda = 15°$–$35°$.

of [15], obtaining good agreement. Table 2 shows the comparison results for $Ra = 10^6$ and $\varepsilon = 0.5$, for Nu_{rad}, the maximum percentage difference was 5.31%; and for Nu_{conv}, the minimum percentage difference was 0.63% for $Ra = 2 \times 10^6$ and $\varepsilon = 0$.

4. Results and discussion

In order to highlight the interaction between the two modes of heat transfer, natural convection and surface thermal radiation in tilted slender cavities, two cases were considered:

- The first case considers the uncoupled mode of heat transfer in a slender cavity. Here, natural convection at the fluid is solved without taking into account the surface thermal radiation and then the surface radiation exchange is solved without taking into account the effect of the natural convection flow in the slender cavity (Uncoupled case). Here, the temperature values on the adiabatic walls were the ones obtained from the natural convection solution equations (1)–(4).
- The second case considers the coupled mode of heat transfer in a slender cavity, that is, the surface radiation is coupled with the natural convection flow (Coupled case).

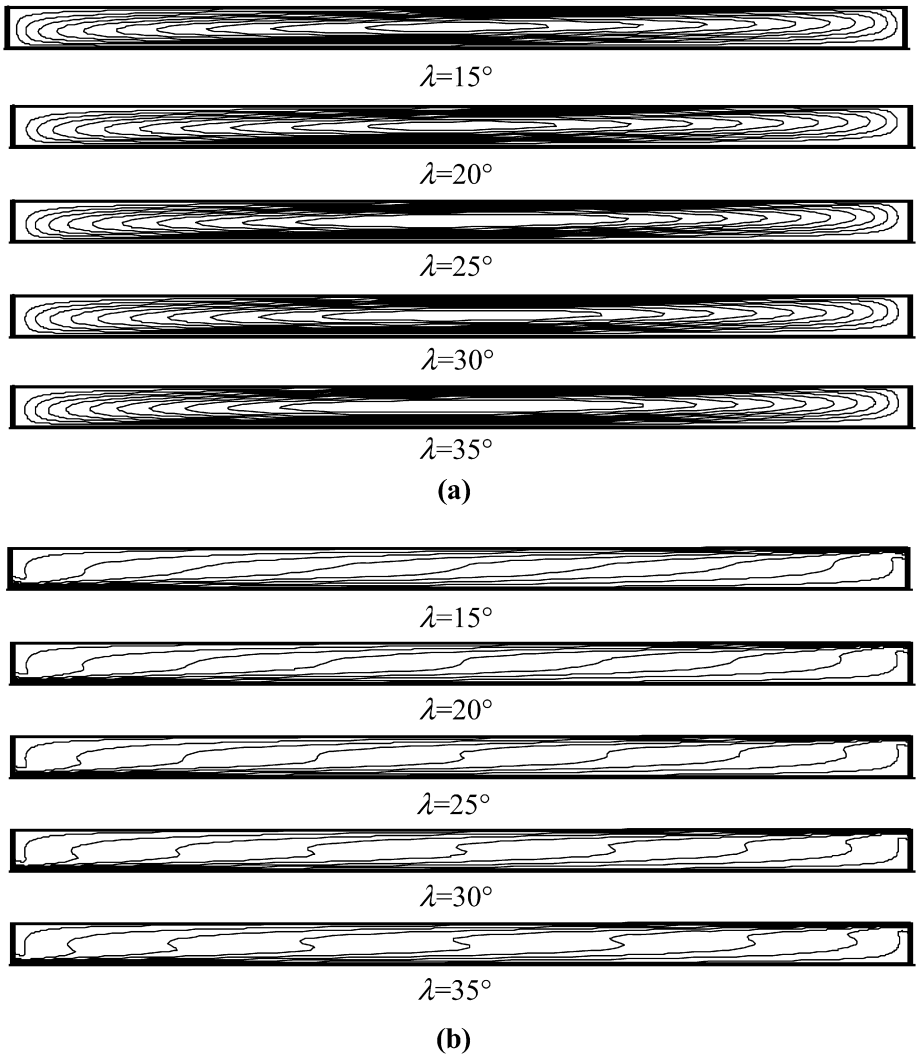

Fig. 3. Case uncoupled—streamlines (a) and isotherms (b) for a cavity of $A = 16$, $Ra = 10^5$ for $\lambda = 15°$–$35°$.

In both cases; streamlines, isotherms and Nusselt numbers in a slender cavity of $A = 16$ and Rayleigh numbers of 10^4, 10^5 and 10^6 are presented. The inclination angle varies from 15° to 35° with increments of 5°. Results presented here include a detail description of the streamline and isotherm plots for $A = 16$, variation of the convection, radiation and total Nusselt numbers of cavities with different aspect ratios, inclination angles, for Ra in the range of 10^4, 10^5 and 10^6; and local heat fluxes of the hot and cold walls for $Ra = 10^6$ and $A = 16$ for the uncoupled and coupled cases.

4.1. Uncoupled case

Figs. 2–4 show streamlines and isotherms for cavities of $A = 16$, in the range of $10^4 \leqslant Ra \leqslant 10^6$ and inclination angles in the range of 15°–35° for the uncoupled case. For each Ra, five sets of streamlines and isotherms are plotted by increasing the inclination angle from 15°–35° at intervals of 5°. The effect of the inclination angle and Ra numbers on natural convection and the uncoupled surface radiation is shown for the highest aspect ratio ($A = 16$).

Visual examination of the flow patterns reveal that for $Ra = 10^4$, the streamlines of Fig. 2 show a nine-cell structure for inclination angle of $\lambda = 15°$ and the isotherms show four thermal plumes. As the inclination angle increases up to $\lambda = 20°$, the number of cells increases to eleven and five-thermal plumes appear, that is due to the increase of heat transfer in the cavity. When the slender cavity rises to $\lambda = 25°$, the multi-cell structure decreases to five cells and also the isotherms decrease to two thermal plumes. For inclination angles of 30° and 35° the multi-cells structure changes into single-cell structure, due to the stronger upslope flows along the x-direction and the thermal plumes disappear showing a conductive thermal boundary layer at the core region of the slender cavity. This transition of the flow pattern (flow mode) strongly depends on the competition of the buoyant flow and the shear flow (along the heating and cooling walls) due to the inclination. The multi-cell structures exist at low inclination angles; whereas a single-cell mode prevails at high inclination angles (the strong longitudinal x-direction flow destroys the multi-cell structures). As the Ra increases from 10^4 to 10^5, the multi-cell structure of the streamlines and the thermal plumes disappears, see Fig. 3, and only the

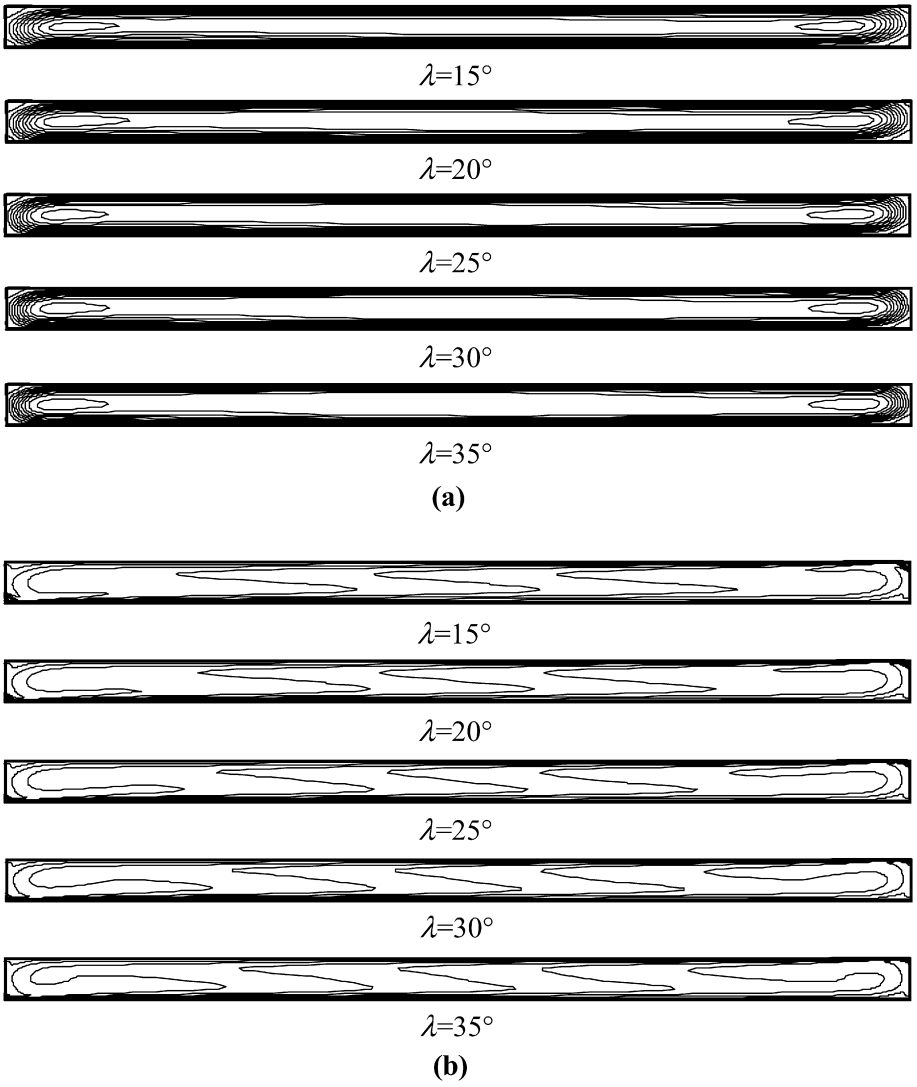

Fig. 4. Case uncoupled—streamlines (a) and isotherms (b) for a cavity of results for $A = 16$, $Ra = 10^6$ for $\lambda = 15°$–$35°$.

unicellular structure is formed because the buoyant forces get stronger for $Ra = 10^5$ rather than for $Ra = 10^4$. The isotherms indicate an increase in the heat transfer. Finally, the streamlines of Fig. 4 for $Ra = 10^6$ show two-in-one main cells for the range of 15° to 35°, those sub-cells are closer to the hot and cold walls. The two sub-cells rotate in the same direction as the main cell. As the inclination angle increases, a very thin boundary-layer is formed because large velocities and temperature gradients appear near to the isothermal walls. As it can be observed, the flow regimes of multi-cell structures disappeared when *Ra* is increased.

4.1.1. Convective and radiative Nusselt numbers (uncoupled case)

Fig. 5 presents the mean convective, radiative and total Nusselt numbers ($Nu_{conv} + Nu_{rad}$) at the hot wall for: (a) $Ra = 10^4$, (b) $Ra = 10^5$ and (c) $Ra = 10^6$ as a function of the inclination angle for aspect ratios of 8, 12, and 16. It can be observed, for all cases, that the Nusselt numbers increases when the Rayleigh number increases. Even though, the radiative *Nu* number increases for different *Ra* numbers, it remains constant with the inclination angles, meaning that the radiative *Nu* number is affected by the geometry of the cavity, that is the size of the walls of the cavity changed with *Ra* number and not with the inclination angle as we expected. Fig. 5(a) shows that for $Ra = 10^4$ and $A = 8$, the total Nusselt number remains almost constant between the angles of 15° to 25°, and decreases for angles of 30° and 35°. But for $Ra = 10^4$ and $A = 12$, the total Nusselt number decreases for all angles. However, for $Ra = 10^4$ and $A = 16$, the Nusselt number slightly increases for the inclination angle of 20° and then decreases. This change is due to the change in the flow pattern from a multi-cell structure to a single-cell structure. As the aspect ratio increases, the mean convective and total Nusselt number decreases, except for $17° < \lambda < 30°$ for $Ra = 10^4$ and $A = 16$. In Figs. 5(b) for $Ra = 10^5$ and 5(c) for $Ra = 10^6$, the mean convective and total Nusselt number increases with the inclination angle except for $A = 8$, $Ra = 10^5$ and $30° < \lambda < 35°$. That is due to the change in the flow pattern from a multi-cell structure to a single-cell structure. However, as we expected, the radiative Nusselt number remains almost

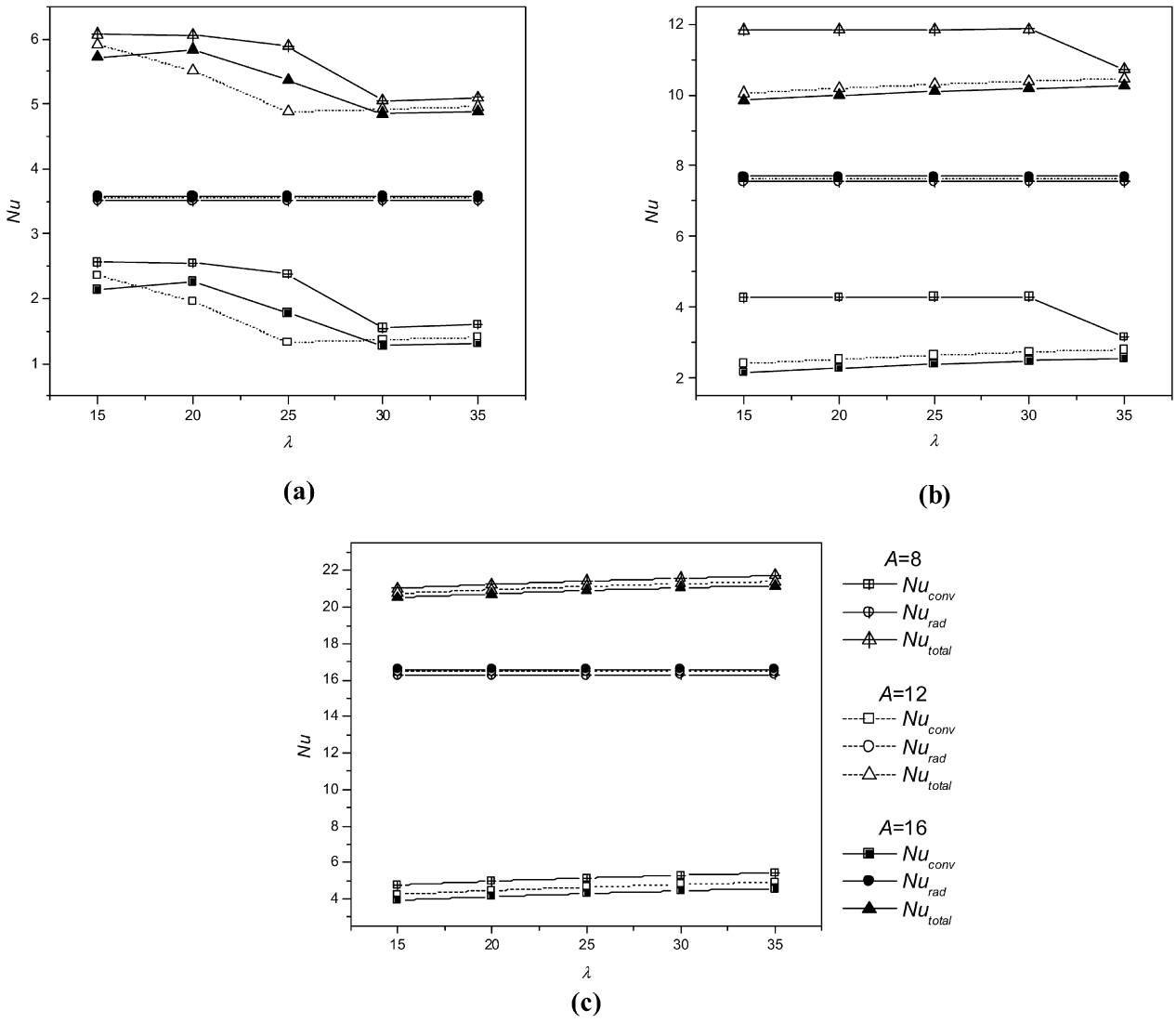

Fig. 5. Case uncoupled—convective, radiative and total Nusselt number in the hot wall as a function of the inclination angle for $A = 8$, 12 and 16 for: (a) $Ra = 10^4$, (b) $Ra = 10^5$ and (c) $Ra = 10^6$.

constant for all angles and aspect ratios, and it increases as the Rayleigh number increases. Also, the higher contribution of the radiative Nusselt number to the total heat transfer is around 72% for $Ra = 10^6$.

4.2. Coupled case

Isotherms and streamlines for the coupled case are illustrated in Figs. 6–8. As in Figs. 2–4, for each *Ra*, five sets of streamlines and isotherms are plotted by increasing the inclination angle from 15°–35°at an intervals of 5°, for the highest aspect ratio ($A = 16$).

As we can appreciate, for $Ra = 10^4$, the streamlines of Fig. 6 show an eleven-cell structure for the inclination angle of $\lambda = 15°$, while the isotherms show five thermal plumes. Contrary to the uncoupled case, as the inclination angle increases to $\lambda = 20°$, the number of cells decreases to nine cells and the isotherms show four thermal plumes. The three-cell structure appears for $\lambda = 25°$ and $\lambda = 30°$ in which the right hand cell is very large. The corresponding isotherms present one thermal plume at the corner of the slender cavity. For $\lambda = 35°$, the streamlines indicate that the multi-cell structure modifies into a single-cell structure due to stronger upslope flows along the x-direction and the heat transfer decreases. Similarly, in Figs. 7 and 8, for $Ra = 10^5$ and $Ra = 10^6$, the streamlines show that the multi-cell structure remains for the inclination angles from 15° to 30°, contrary to the uncoupled case (Figs. 3 and 4). For $Ra = 10^5$ and $\lambda = 15°$, Fig. 7(a) shows that a seven-cell structure is produced, as the λ increases up to 30° the multicellular structure changes to a five-cell structure. For $\lambda = 35°$, a three-cell structure is formed: a main cell that occupies almost 90% of the cavity, and two smaller cells located at the sides of the main cell. The two cells are moving clockwise and the main one is moving counterclockwise. The isotherm figures show thermal plumes for the inclination range of 15° to 30° which indicate a highly convective regime. For $\lambda = 35°$, a very thin thermal boundary layer appears at the isothermal hot and cold walls. In $Ra = 10^6$, the streamlines of Fig. 8

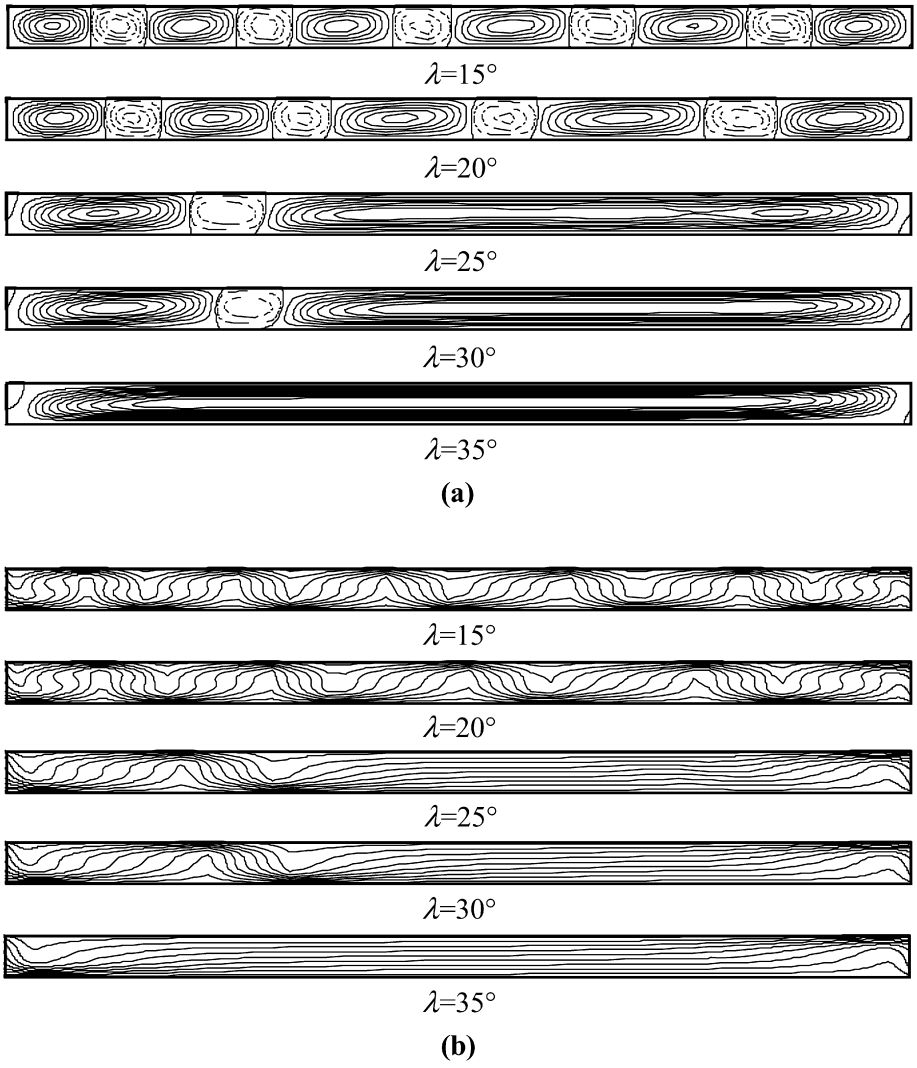

Fig. 6. Case coupled—streamlines (a) and isotherms (b) for a cavity of $A = 16$, $Ra = 10^4$ for $\lambda = 15°$–$35°$.

show that the multi-cell structure and the thermal plumes continue for inclination angles in the range of 15°–30°. When $\lambda = 35°$ a three-in-one cell structure streamlines is observed. Comparing the uncoupled case against the coupled case we can see that the coupling convection and surface radiation modify the flow patterns and the temperature distributions at the walls, because the multi-cell structure appears for all *Ra* and $15° < \lambda < 35°$.

4.2.1. Convective and radiative Nusselt numbers (coupled case)

Fig. 9 presents the variation of the mean convective, Nu_{conv}, the radiative, Nu_{rad}, and the total Nusselt numbers at the hot wall, $Nu_{total} = Nu_{con} + Nu_{rad}$, for: (a) $Ra = 10^4$, (b) $Ra = 10^5$ and (c) $Ra = 10^6$ as a function of the inclination angles for aspect ratios of 8, 12, and 16. Similarly to the Uncoupled case, we can see that all the Nusselt numbers increase when the Rayleigh number increases. Also the Nu_{rad} increases with *Ra* but it remains constant as the inclination angle increases, as it was expected, because the radiative Nusselt number depends on the dimensions of the cavity. When $Ra = 10^4$ and $A = 8$, 12 the Nu_{conv} and Nu_{total} does not change between the inclination angles of 15° to 25°. However, for $A = 16$, the Nu_{convl} and Nu_{total} decreases to a minimum in $\lambda = 25°$ and then slightly increases but decreases again, see Fig. 9(a). In Fig. 9(b) for $A = 8$ and 12, the Nu_{conv} and Nu_{total} remain almost constant up to $\lambda = 30°$ and decreases afterwards, because the flow change from multicellular to unit-cell pattern, but for $A = 16$, the Nu_{conv} and Nu_{total} slightly oscillates and then decreases for $\lambda = 35°$. Finally, in a similar way for $Ra = 10^6$, the mean convective and total Nusselt number increase, except when the flow patterns change from multi-cell to unit-cell pattern. As the aspect ratio increases, the convective and total Nusselt number decreases for $Ra = 10^4$ to 10^6, except for $A = 16$ and $Ra = 10^6$. For $Ra = 10^6$, the radiative Nusselt number contributes around 70% to the total heat transfer in the slender cavity.

Comparing the mean Nusselt number results of Figs. 5 and 9, it is observed that when the mean convective and radiative modes of heat transfer are uncoupled, the *Nu* numbers can be over or under estimated. Table 3 shows the maximum percentage difference of the over-estimated and under-estimated values of the Nu_{conv} and Nu_{rad} at the hot wall for $Ra = 10^4$, 10^5

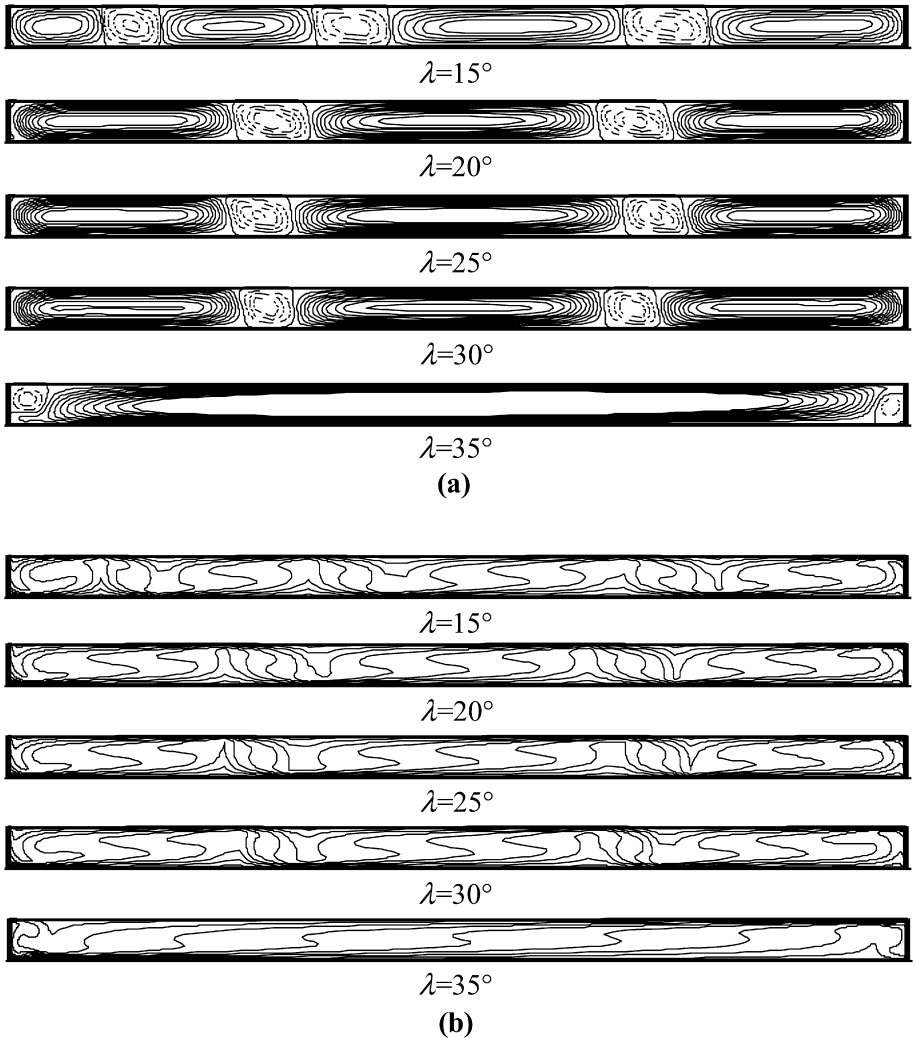

Fig. 7. Case coupled—streamlines (a) and isotherms (b) for a cavity of $A = 16$, $Ra = 10^5$ for $\lambda = 15°$–$35°$.

and 10^6. For $Ra = 10^4$, the Nu_{conv} is overestimated by 18.76%, when $A = 16$ and $\lambda = 25°$, and underestimated by 39.94%, when $A = 12$ and $\lambda = 25°$. For $Ra = 10^5$, the Nu_{conv} is overvalued by 19.66% for $A = 8$ and $\lambda = 30°$, and under-estimated by 37.02% for $A = 16$ and $\lambda = 15°$. For $Ra = 10^6$, the Nu_{conv} is overestimated by 3.07% for $A = 8$ and $\lambda = 35°$ and underestimate by 25.12% for $A = 16$ and $\lambda = 15°$. On the other hand, it is observed that the radiative Nusselt number is overestimated less than 1% in all cases analyzed.

4.3. Radiative heat fluxes

Fig. 10 shows the local radiative heat fluxes on the adiabatic walls, for the uncoupled case and the coupled case, as a function of the inclination angle, for $A = 16$ and $Ra = 10^6$. We can appreciate that the local radiative heat fluxes are almost symmetrical for the uncoupled case (Fig. 10(a)). For the coupled case, the local radiative heat fluxes are not symmetrical, also, as it is shown in Fig. 10(b), we can see, that the radiative flux does not change significantly with the inclination angle. The average radiative heat fluxes on the walls and the total radiative balance in the cavity ($q_{total} = q_S + q_N + q_E + q_W$), for the uncoupled and coupled cases, for $A = 16$, $\lambda = 15°$, $Ra = 10^4$, 10^5 and 10^6, are summarized in Table 4. The average radiative heat fluxes from the isothermal walls (q_S and q_N) are similar for the uncoupled and coupled cases; the maximum percentage difference is less than 1%. However, the average radiative heat fluxes on the adiabatic walls (q_E and q_W) show that there is a significant reduction in the average radiative heat fluxes, when the surface radiation is coupled with the natural convec-

Table 3
Maximum percentage difference between the over-estimate and under estimate values of Nu_{conv} and Nu_{rad} in the hot wall

Ra	Convective Nusselt number		Radiative Nusselt number
	Over-estimate (Case)	Under-estimate (Case)	Over-estimate (Case)
10^4	18.76% ($A = 16$, $\lambda = 25°$)	39.94% ($A = 12$, $\lambda = 25°$)	0.91% ($A = 16$, $\lambda = 15°$)
10^5	19.66% ($A = 8$, $\lambda = 30°$)	37.02% ($A = 16$, $\lambda = 15°$)	0.54% ($A = 8$, $\lambda = 15°$)
10^6	3.07% ($A = 8$, $\lambda = 35°$)	25.12% ($A = 16$, $\lambda = 15°$)	0.68% ($A = 8$, $\lambda = 35°$)

Note. The parameters in ( ) are the cases where is presented the maximum percentage difference.

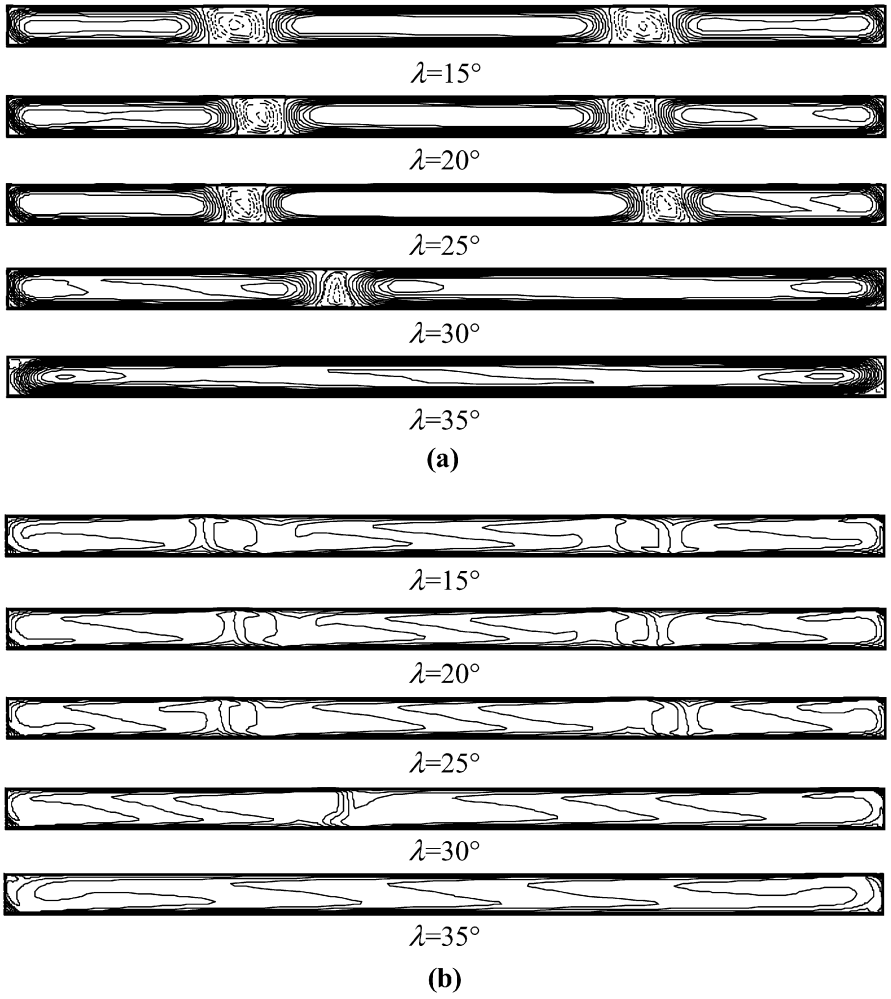

Fig. 8. Case coupled—streamlines (a) and isotherms (b) for a cavity of results for $A = 16$, $Ra = 10^6$ for $\lambda = 15°$–$35°$.

Table 4
Average radiative heat fluxes for $A = 16$ and $\lambda = 15°$ for Rayleigh numbers of 10^4, 10^5 and 10^6

Ra	q_S (W m^{-2})	q_W (W m^{-2})	q_N (W m^{-2})	q_E (W m^{-2})	q_{total} (W m^{-2})
Case uncoupled					
10^4	76.033	−1.703	−75.202	0.875	0.003
10^5	163.678	−4.858	−162.147	3.332	0.005
10^6	352.821	−8.068	−349.140	4.403	0.016
Case coupled					
10^4	75.861	−0.843	−75.347	0.331	0.002
10^5	163.306	−1.742	−162.454	0.893	0.003
10^6	351.777	−3.072	−350.045	1.349	0.009

Table 5
Average radiative heat fluxes for $Ra = 10^6$ and $\lambda = 15°$ for aspect ratios of 8, 12 and 16

Ra	q_S (W m^{-2})	q_W (W m^{-2})	q_N (W m^{-2})	q_E (W m^{-2})	q_{total} (W m^{-2})
Case uncoupled					
8	172.919	−7.829	−169.288	4.212	0.014
12	262.835	−8.031	−259.181	4.392	0.015
16	352.821	−8.068	−349.140	4.403	0.016
Case coupled					
8	171.883	−3.111	−170.247	1.481	0.006
12	261.774	−3.080	−260.120	1.432	0.006
16	351.777	−3.072	−350.045	1.349	0.009

tion. The maximum percentage difference was 273% for the adiabatic wall, q_E, for $Ra = 10^5$.

Table 5 illustrates the average radiative heat fluxes and the total radiative balance in the cavity ($q_{\text{total}} = q_S + q_N + q_E + q_W$) at high $Ra = 10^6$ and $\lambda = 15°$ for different aspect ratios, $A = 8$, 12 and 16. It is shown that, as in the previous case, the average radiative heat fluxes from the isothermal walls (q_S and q_N) are very similar; with a maximum difference less than 1%. However, there is a significant reduction of the average radiative heat fluxes on the adiabatic walls (q_E and q_W), when the coupled case is considered. The maximum percentage difference was 226% for the adiabatic wall, q_E, for $A = 16$.

4.4. Nusselt number correlation

For the coupled case, a correlation equation for the total Nusselt number as a function of Ra number, the inclination angle and the aspect ratio is presented. To obtain this correlation,

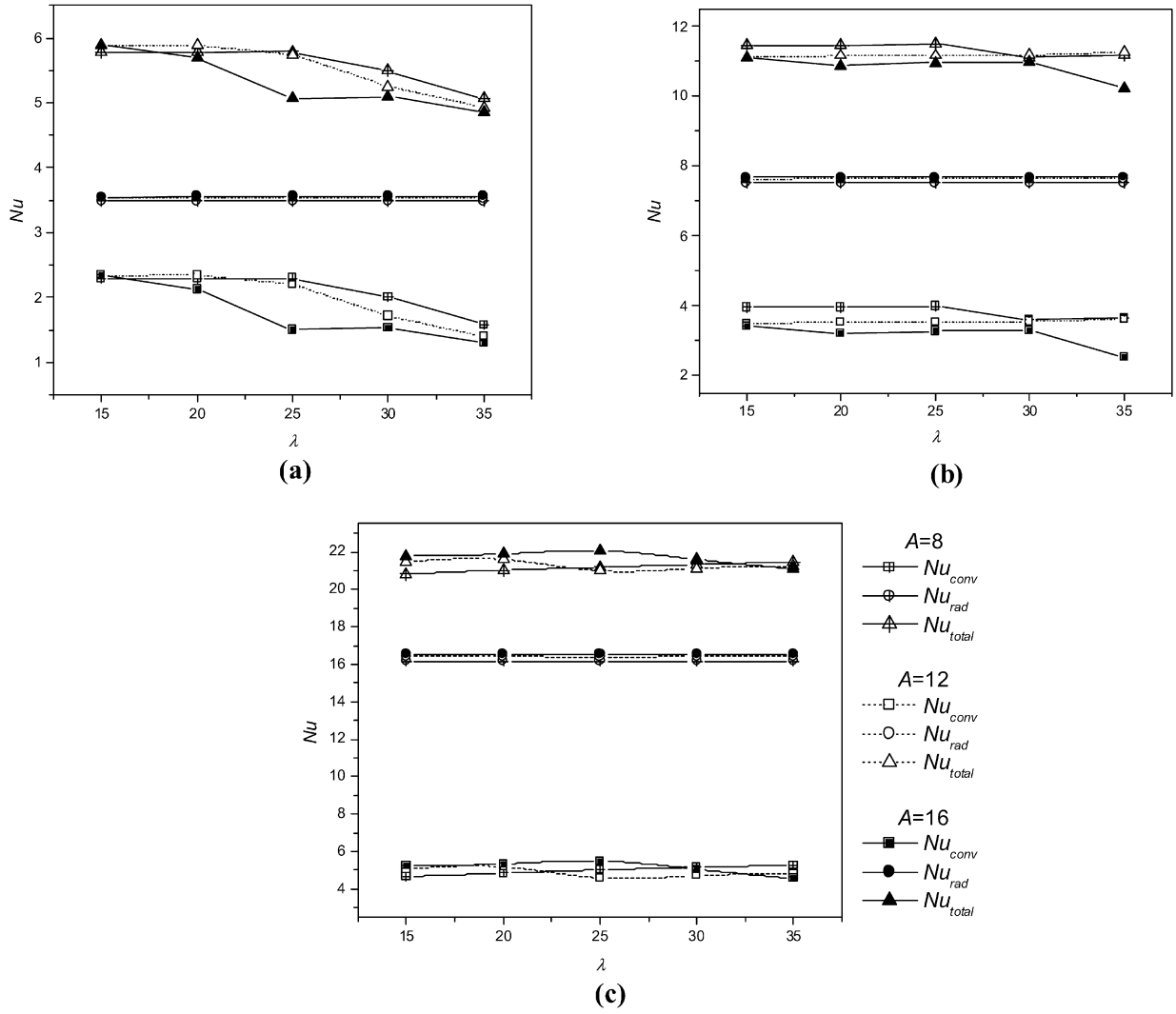

Fig. 9. Case coupled—convective, radiative and total Nusselt number in the hot wall as a function of the inclination angle for $A = 8$, 12 and 16 for: (a) $Ra = 10^4$, (b) $Ra = 10^5$ and (c) $Ra = 10^6$.

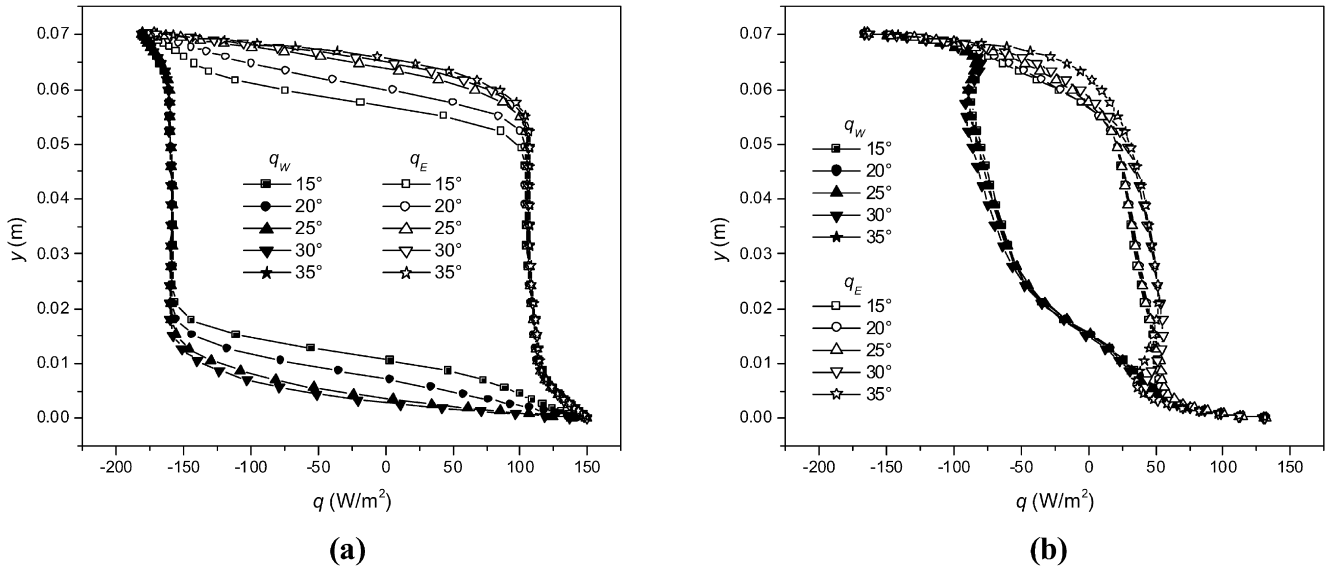

Fig. 10. Local radiative heat fluxes on the inner walls for $A = 16$, $Ra = 10^6$: (a) Case uncoupled, (b) Case coupled.

Table 6
Functions $f_1(\lambda)$ and $f_2(\lambda)$ for the fitted equation (12)

A	Ra	$f_1(\lambda)$	$f_2(\lambda)$
8	10^4–10^5	$(\sin 5\lambda)^{0.38}$	1
8	10^6	1	$0.8(\sin\lambda)^{0.35}$
12	10^4	$1.1(\sin 4.7\lambda)$	0
12	10^5–10^6	1	$0.65(\sin\lambda)^{0.1}$
16	10^4–10^6	$(1-\frac{1708\sin 137\lambda}{Ra\cos\lambda})\cos 2.15\lambda$	$0.87(\sin 3.4\lambda)$

a method described by [24] was used. The *Nu* number correlation has four terms corresponding to: conduction regime (I), convection regime (II), and the boundary layer regime (III) and (IV) the contribution of surface radiation. Thus, the total Nusselt number correlation is described as:

$$Nu_{\text{total}} = \underbrace{1}_{\text{I}} + \underbrace{1.44\left[1-\frac{1708}{Ra\cos\lambda}\right]^{*} f_1(\lambda)}_{\text{II}} + \underbrace{\left[\left(\frac{Ra\cos\lambda}{5830}\right)^{1/3}-1\right]^{*} f_2(\lambda)}_{\text{III}} + \underbrace{0.171(Ra\cos\lambda)^{0.333}}_{\text{IV}} \tag{12}$$

the brackets $[\,]^*$ indicates that the value must set equal to zero if it becomes negative. The terms (II) and (III) are multiplied by the functions $f_1(\lambda)$ and $f_2(\lambda)$ respectively. Table 6 shows the $f_1(\lambda)$ and $f_2(\lambda)$ that were calculated fitting the numerical values of the *Nu* number. The maximum percentage difference between the numerical and the fitted values computed was close to 6% and the average percentage difference is close to 2%.

5. Conclusions

This paper presented a numerical study of the interaction between the heat transfer by natural convection and surface thermal radiation in a tilted slender cavity. The parameters analyzed were the *Ra* number in the range of 10^4–10^6, the aspect ratios 8, 12 and 16 and the inclination angles in the range of 15°–35°.

For the uncoupled and coupled cases, the behavior of the isotherms and streamlines was different; so the decoupling of two modes of heat transfer for $A = 8$, 12 and 16 and inclination angles range of $15° \leqslant \lambda \leqslant 35°$ is not possible; different thermal plumes and a multi-cell flow streamlines were observed in both cases. For the uncoupled case, the increase of the aspect ratio and/or the increase of the Rayleigh number reduce the buoyancy forces, so the multi-cell pattern disappears. But for the coupled case, buoyancy forces raise and the multi-cell patterns were observed in most cases.

For the uncoupled case, the radiative heat fluxes on the adiabatic walls are almost symmetrical; contrary to the coupled case; in which there is a reduction of the mean radiative heat fluxes of approximately 200% on the adiabatic walls. It was found that the radiative heat transfer mode contributes by almost 72% of total heat transfer for the uncoupled case, and 70% when both heat transfer mechanisms are coupled.

A correlation equation for the total Nusselt number as a function of the Rayleigh number, and the inclination angle is presented for each aspect ratio. This correlation can be useful in the design of solar collectors located in latitudes between 35° and 15°.

Finally, this study demonstrated the importance of considering the coupling of the two modes of heat transfer; natural convection and surface thermal radiation in tilted slender cavities.

Acknowledgement

The authors are grateful to Consejo del Sistema Nacional de Educación Tecnológica (COSNET) and the Secretaria de Educación Pública (SEP), whose financial support made this work possible.

References

[1] G.N. Ivey, Experiments on transient natural convection in a cavity, J. Fluid Mech. 144 (1984) 389–401.
[2] S. Ostrach, Natural convection in enclosures, J. Heat Transfer 110 (1988) 1175–1190.
[3] S. Paolucci, D.R. Chenoweth, Natural convection in shallow enclosures with differentially heated endwalls, J. Heat Transfer 110 (1988) 625–634.
[4] H. Ozoe, H. Sayama, S. Churchill, Natural convection in an inclined square channel, Int. J. Heat Mass Transfer 17 (1974) 401–406.
[5] H. Ozoe, H. Sayama, S. Churchill, Natural convection in an inclined rectangular channel at various aspect ratios and angles—experimental measurements, Int. J. Heat Mass Transfer 18 (1975) 1425–1431.
[6] R. Rahman, M.A. Sharif, Numerical study of laminar natural convection in inclined rectangular enclosures of various aspect ratios, Numer. Heat Transfer Part A 44 (2003) 355–373.
[7] D.W. Larson, R. Viskanta, Transient combined laminar free convection and radiation in a rectangular enclosure, J. Fluid Mech. 78 (1976) 65–85.
[8] L.C. Chang, K.T. Yang, J.R. Lloyd, Radiation-natural convection interactions in two-dimensional complex enclosures, J. Heat Transfer 105 (1983) 89–95.
[9] C. Balaji, S.P. Venkateshan, Correlations for free convection and surface radiation in a square cavity, Int. J. Heat Fluid Flow 15 (1994) 249–252.
[10] M. Akiyama, Q.P. Chong, Numerical analysis of natural convection with surface radiation in a square enclosure, Numer. Heat Transfer Part A 31 (1997) 419–433.
[11] S.K. Mahapatra, S. Sen, A. Sarkar, Interaction of surface radiation and variable property natural convection in a differentially heated square cavity—a finite element analysis, Int. J. Num. Meth. Heat Fluid Flow 9 (1999) 423–443.
[12] N. Ramesh, S.P. Venkateshan, Effect of surface radiation on natural convection in a square enclosure, J. Thermophys. Heat Transfer 13 (1999) 299–301.
[13] C.Y. Soong, P.Y. Tzeng, D.C. Chiang, T.S. Sheu, Numerical study on mode-transition of natural convection in differentially heated inclined enclosures, Int. J. Heat Mass Transfer 39 (1996) 2869–2882.
[14] P.Y. Tzeng, C.Y. Soong, T.S. Sheu, Numerical investigation of transient flow-mode transition of laminar natural convection in an inclined enclosure, Numer. Heat Transfer Part A 31 (1997) 193–206.
[15] E.H. Ridouane, M. Hasnaoui, A. Amahmid, A. Raji, Interact between natural convection and radiation in a square cavity heated from below, Numer. Heat Transfer Part A 45 (2004) 289–311.
[16] G. Colomer, M. Costa, R. Cónsul, A. Oliva, Three-dimensional numerical simulation of convection and radiation in a differentially heated cavity using the discrete ordinates method, Int. J. Heat Mass Transfer 47 (2004) 257–269.

[17] E.H. Ridouane, M. Hasnaoui, A. Campo, Effect of surface radiation on natural convection in a Rayleigh–Benard square enclosure: steady and unsteady conditions, Heat Mass Transfer 42 (2006) 214–225.
[18] C. Balaji, S.P. Venkateshan, Combined surface radiation and free convection in cavities, J. Thermophys. Heat Transfer 8 (1994) 373–376.
[19] K. Velusamy, T. Sundararajan, K. Seetharamu, Interaction effects between surface radiation and turbulent natural convection in square and rectangular enclosures, J. Heat Transfer 123 (2001) 1062–1070.
[20] J.A. Duffie, W.A. Beckman, Solar Engineering of Thermal Processes, John Wiley & Sons Publications, New York, 1991.
[21] M.F. Modest, Radiative Heat Transfer, McGraw–Hill, New York, 1993.
[22] S.V. Patankar, Numerical Heat Transfer and Fluid Flow, Taylor and Francis, London, 1980.
[23] J.P. Van Doormaal, G.D. Raithby, Enhancement of the SIMPLE method for predicting incompressible fluid flows, Numer. Heat Transfer Part A 7 (1984) 147–163.
[24] K.G. Hollands, T.E. Unny, G.D. Raithby, L. Konicek, Free convective heat transfer across inclined air layers, ASME J. Heat Transfer 98 (1976) 189–193.